

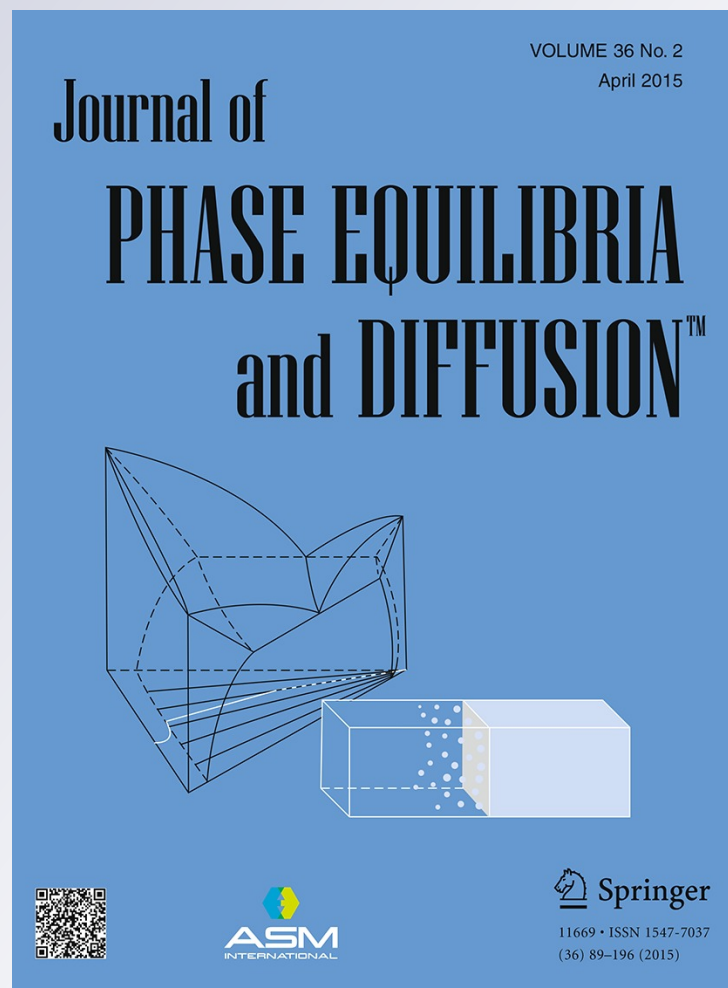
# *Reactions Between $Ti_2AlC$ , $B_4C$ , and Al and Phase Equilibria at 1000 °C in the Al- Ti-B-C Quaternary System*

**Matthias T. Agne, Babak Anasori &  
Michel W. Barsoum**

**Journal of Phase Equilibria and  
Diffusion**

ISSN 1547-7037  
Volume 36  
Number 2

J. Phase Equilib. Diffus. (2015)  
36:169-182  
DOI 10.1007/s11669-015-0371-9



**Your article is protected by copyright and all rights are held exclusively by ASM International. This e-offprint is for personal use only and shall not be self-archived in electronic repositories. If you wish to self-archive your article, please use the accepted manuscript version for posting on your own website. You may further deposit the accepted manuscript version in any repository, provided it is only made publicly available 12 months after official publication or later and provided acknowledgement is given to the original source of publication and a link is inserted to the published article on Springer's website. The link must be accompanied by the following text: "The final publication is available at [link.springer.com](http://link.springer.com)".**

# Reactions Between $Ti_2AlC$ , $B_4C$ , and Al and Phase Equilibria at 1000 °C in the Al-Ti-B-C Quaternary System

Matthias T. Agne, Babak Anasori, and Michel W. Barsoum

(Submitted November 8, 2014; in revised form January 21, 2015; published online February 27, 2015)

As automotive, aerospace and the power industries increasingly look to carbide and boride based aluminum, Al, composites for their high specific strengths and increased thermal stability, it is important to characterize the equilibrium phase relations at temperatures common for processing these composites. Herein, two composites were fabricated starting with Al,  $Ti_2AlC$ , and  $B_4C$ . The  $Ti_2AlC/B_4C$  powders were mixed in both 50/50 and 75/25 vol.% ratios and cold pressed into 53% dense preforms. The preforms were pressureless melt infiltrated in the 900–1050 °C temperature range with Al. Ten hour equilibration experiments were also conducted at 1000 °C. X-ray diffraction and scanning electron microscopy confirmed that neither  $Ti_2AlC$  nor  $B_4C$  was an equilibrium phase. A number of reaction phases— $AlB_2$ ,  $Al_3BC$ ,  $TiB_2$ ,  $TiC$ ,  $TiAl_3$  and  $Al_4C_3$ —could be found in the non-equilibrated samples. However, the equilibrium phases were found to be Al,  $TiB_2$ ,  $Al_3BC$ , and  $Al_4C_3$  for the more B-rich composite and Al,  $TiB_2$ ,  $TiC$ , and  $Al_4C_3$  for the Ti-rich composite. From these results, the 1000 °C quaternary phase diagram adjacent to the Al- $TiB_2$ - $Al_4C_3$  triangle and in the Al-rich corner was developed for the first time. This study is a requisite first step for the development and use of advanced composites in the Al-Ti-B-C system.

**Keywords** aluminum, equilibria, MAX phase, MMCs, phase diagram

## 1. Introduction

### 1.1 Background

Metal matrix composites, MMCs, attempt to combine the advantageous properties of both metals and ceramics. Wear resistance, fatigue and fracture resistance, and reduced coefficient of thermal expansion (compared to the metal matrix) are attractive reasons to incorporate ceramic reinforcements into metal matrices, while retaining the good thermal and electrical conductivities, and machinability of metals.<sup>[1]</sup> Mixing of a metal, or alloy, with a reinforcement phase may be achieved through a variety of processes such as stir casting, melt infiltration, powder metallurgy, among others.<sup>[1]</sup> Common ceramic reinforcements include:  $Al_2O_3$ ,  $SiC$ ,<sup>[2]</sup>  $B_4C$ ,<sup>[3]</sup>  $TiC$ ,<sup>[4]</sup> and  $TiB_2$ .<sup>[5]</sup> A more thorough review of MMCs and their properties may be found elsewhere.<sup>[1,6]</sup>

Al-matrix composites reinforced with titanium carbide,  $TiC$ , and/or boron carbide,  $B_4C$ , have been targeted as families of lightweight materials with the potential to operate at temperatures above those of Al and its alloys. The

high hardness typical of boride and carbide-containing composites also makes them attractive for high wear applications. Their chemical stability and neutron absorption properties render them appealing in nuclear and other demanding industrial settings.<sup>[7,8]</sup>

Recently, magnesium, Mg, matrix composites reinforced with  $Ti_2AlC$ —a member of the MAX phases—have been developed.<sup>[9–11]</sup> The MAX are a family of nanolayered, machinable, ternary carbides and nitrides, having the general formula  $M_{n+1}AX_n$ —where  $n = 1, 2, 3$ ; M is an early transition metal; A is an A-group element (mostly groups 13 and 14); and X is C and/or N.<sup>[12]</sup> The MAX phases combine some of the best properties of metals and ceramics. Like metals they are machinable, electrically and thermally conductive,<sup>[13,14]</sup> damage tolerant and not susceptible to thermal shock.<sup>[15]</sup> Like ceramics, some of them are lightweight ( $\approx 4 \text{ Mg/m}^3$ ) and elastically rigid (Young's moduli  $> 300 \text{ GPa}$ ).  $Ti_2AlC$  is also creep, fatigue and oxidation resistant.<sup>[12,16–18]</sup>

The aforementioned Mg and Mg alloys-MAX composites were manufactured by spontaneous melt infiltration, MI, at relatively low processing temperatures (750 °C) yielding composites with attractive mechanical properties. For example, the Young's modulus and ultimate compressive strengths, UCSs, of a Mg alloy (AZ61) matrix composite reinforced with 50 vol.%  $Ti_2AlC$  particles were measured to be  $136 \pm 6 \text{ GPa}$  and  $760 \pm 9 \text{ MPa}$ , respectively. In addition to the excellent mechanical properties, these composites can also dissipate almost 25% of the applied mechanical energy at high stresses.<sup>[11,19]</sup> Furthermore, the resulting composites were also most readily machinable, since both components are machinable. These promising results spurred interest in developing Al-MAX composites with comparable or better properties using MI.

Electronic supplementary material The online version of this article (doi:10.1007/s11669-015-0371-9) contains supplementary material, which is available to authorized users.

Matthias T. Agne, Babak Anasori, and Michel W. Barsoum, Department of Materials Science and Engineering, Drexel University, Philadelphia, PA 19104, USA. Contact e-mail: mta37@drexel.edu.

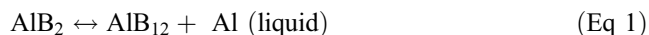
Fabricating Al-matrix MAX reinforced composites is complicated by the fact that Al is not in equilibrium with most MAX phases.<sup>[12]</sup> For example, Wang et al.<sup>[20]</sup> attempted to fabricate  $Ti_3AlC_2$  composites at elevated temperatures and found that above 950 °C,  $Ti_3AlC_2$  reacted with Al to form TiC and  $TiAl_3$ . To circumvent this problem Wang et al.<sup>[20]</sup> hot pressed Al and  $Ti_3AlC_2$  powders at a temperature (550 °C) at which the reaction kinetics were slow. More recently, Hu et al.<sup>[21]</sup> used current-activated, pressure-assisted infiltration to fabricate Al- $Ti_2AlC$  composites. In this method, the processing and densification occur too rapidly for extensive reactions to occur. Their nearly full dense composites were lightweight with UCS's of the order of 500 MPa. At 160 MPa  $cm^3/g$ , their specific strengths were approximately 4 times higher than those of pure Al.<sup>[21]</sup> These solutions to the problem, however, do not lend themselves to rapid, near-net shape, inexpensive manufacturing.

As noted above, the original goal of this work was to fabricate Al- $Ti_2AlC$  composites via MI. However, preliminary results obtained herein showed that porous  $Ti_2AlC$  preforms were not easily wet by molten Al even at 1000 °C. At higher temperatures, the reaction was quite intense and did not result in a usable material. Poor wetting by Al is not unique to  $Ti_2AlC$ , but is also encountered when fabricating MMCs with other carbides, such as TiC,  $B_4C$  and SiC.<sup>[22]</sup> Typically temperatures greater than 1000 °C are necessary for Al to wet TiC and/or  $B_4C$  preforms in MI experiments.<sup>[3,4]</sup> However, it has been previously reported that Ti additions to  $B_4C$  porous preforms enhance the infiltration kinetics of Al into the latter,<sup>[3]</sup> which coincides with the finding that Ti-B interactions aid in the reactive wetting of Al on ceramic surfaces,<sup>[23]</sup> though the reaction mechanisms and phase equilibria remain largely un-investigated.<sup>[3]</sup> Nevertheless, this interest in manufacturing Al matrix composites with both borides and carbides<sup>[24]</sup> would be greatly aided by an understanding of the reaction mechanisms and especially the equilibrium phase relations of these systems.

This work sought to enhance the infiltration kinetics of Al into  $Ti_2AlC$  at lower temperatures by incorporating  $B_4C$  in the preforms, in an attempt to reduce or eliminate the high temperature reactions observed between  $Ti_2AlC$  and Al. However, when it was found that in all cases, a reaction occurred, the focus of the work shifted to understanding the equilibrium phase relations in the Al-Ti-B-C quaternary system. Before doing so, it is important to review the following phase diagrams.

## 1.2 Binary Phase Diagrams

**1.2.1 Al-B System.** Currently, only the binary phases  $AlB_2$  and  $AlB_{12}$  have been shown to be pure Al-borides.<sup>[25]</sup>  $AlB_2$  is stable to at least  $956 \pm 5$  °C. Above that temperature it peritectically transforms according to<sup>[26]</sup>



Others reported that the transformation temperature may be as high as  $972 \pm 5$  °C.<sup>[27]</sup>  $AlB_{12}$  is stable to  $\approx 2000$  °C. The solubility of B in liquid Al at 1100 °C is about 7 at.%.

**1.2.2 Al-C System.** The only binary phase in the Al-C system is  $Al_4C_3$ . And while this phase has been reported to be stable to above 2100 °C,<sup>[28]</sup> when in contact with  $TiAl_3$  it will react to form TiC and Al at  $\approx 877$  °C.<sup>[29]</sup> The solubility of C in Al is negligible in the temperature range used herein.<sup>[28]</sup>

**1.2.3 Al-Ti System.** A multitude of binary intermetallic phases exist between Al and Ti, that include  $Ti_3Al$ ,  $TiAl$ ,  $Ti_3Al_5$ ,  $TiAl_2$ ,  $Ti_2Al_5$ ,  $Ti_5Al_{11}$ , and  $TiAl_3$ .<sup>[30]</sup> At 1000 °C, the stable phases are:  $\alpha$ -Ti,  $\beta$ -Ti,  $TiAl_3$ ,  $TiAl$ ,  $TiAl_2$ ,  $Ti_2Al_5$ , and  $TiAl_3$ .<sup>[30,31]</sup>

**1.2.4 Ti-B System.** Initial investigations of the Ti-B system suggested the existence of the binary phases  $Ti_2B$  and  $Ti_2B_5$ ,<sup>[32]</sup> however the existence of these phases has since been refuted. The current Ti-B phase diagram, shows only the binary phases  $TiB$ ,  $Ti_3B_4$  and  $TiB_2$ , all of which are stable to  $\approx 2000$  °C.<sup>[33]</sup>

**1.2.5 Ti-C System.** Non-stoichiometric  $TiC_y$  ( $0.47 < y < 1.00$ ) is the only Ti-C binary phase in the Ti-C system. The existence of various ordered phases such as  $Ti_2C$ ,  $Ti_6C_5$ , and  $Ti_3C_2$  have sometimes been reported, however.<sup>[34]</sup>

**1.2.6 B-C System.** Within the B-C system, the only known binary phase is  $B_4C$ , with B-rich (carbon deficient) variations of the form  $B_4C_{1-z}$  ( $0 < z < 0.55$ ).<sup>[32,34]</sup> This phase is thermally stable to nearly 2500 °C. An extensive review of the history, processing, and properties of  $B_4C$  can be found in the literature.<sup>[35]</sup>

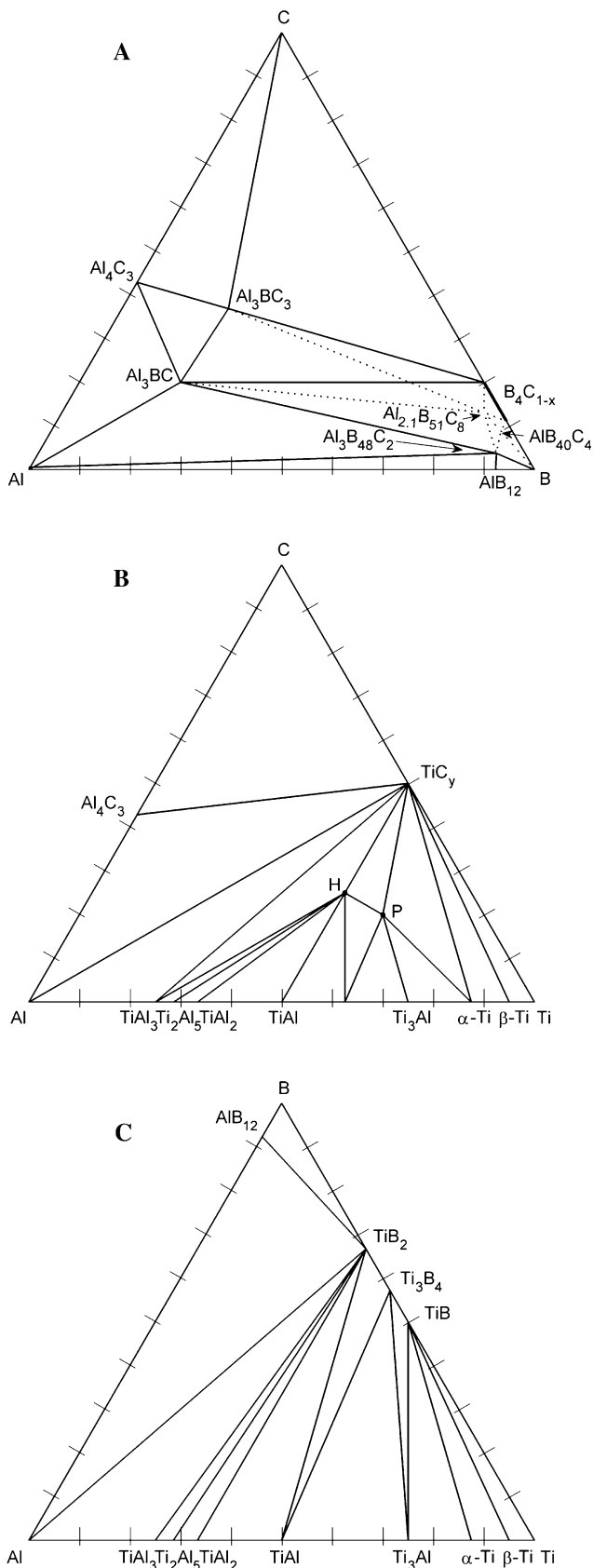
## 1.3 Ternary Phase Diagrams

**1.3.1 Al-B-C.** Figure 1(a) re-plots the Al-B-C ternary phase diagram used herein.<sup>[36]</sup> Some confusion has been associated with the phases reported in the Al-B and Al-B-C systems.<sup>[36]</sup> For example, the existence of stoichiometric  $AlB_{10}$  was first reported,<sup>[37]</sup> but was later shown, by Matkovich et al.,<sup>[38]</sup> to contain carbon such that its chemistry was better described by  $AlB_{24}C_4$ .<sup>[38]</sup>

More than forty phases are known to exist in the Al-B-C system.<sup>[36]</sup> Isothermal experiments carried out at 900, 1000, and 1400 °C have been used to tentatively draw conclusions about equilibrium relations.<sup>[36]</sup> The stable phases reported at 900 °C—including  $Al_4C_3$ ,  $Al_3BC$ ,  $Al_3BC_3$ ,  $Al_3B_{48}C_2$  and  $B_4C$ —remain stable at 1000 °C (Fig. 1a). Since this work deals with the Al rich-corner of the quaternary phase diagram, the only relevant phase is  $Al_3BC$ . The latter is reported to be stable to  $\approx 1100$  °C, after which it reacts with  $AlB_{12}$  to form  $Al_3B_{48}C_2$  and liquid Al.<sup>[36]</sup>

**1.3.2 Al-Ti-C System.** Isothermal sections of the Al-Ti-C system have been extensively investigated over the 727 to 1300 °C temperature range, with reproducibility between studies.<sup>[31]</sup> Of the three ternary phases known to exist, two— $Ti_3AlC_2$  and  $Ti_2AlC$ —belong to the MAX phase family;<sup>[12]</sup> the third,  $Ti_3AlC$ , has a perovskite-type crystal structure.<sup>[30]</sup>

Both  $Ti_2AlC$  and  $Ti_3AlC$  can be found in the ternary system at every temperature between 750 and 1300 °C. However, according to Pietzka and Schuster,<sup>[30]</sup>  $Ti_3AlC_2$  is not an equilibrium phase at, or below, 1000 °C. The equilibrium relations at 1000 °C (Fig. 1b) and 1300 °C



◀ **Fig. 1** Isothermal ternary diagrams at 1000 °C of, (a) Al-B-C system as presented by Grytsiv;<sup>[36]</sup> (b) Al-Ti-C system as presented by Pietzka and Schuster, where H and P represent the  $Ti_2AlC$  and  $Ti_3AlC$  phases, respectively;<sup>[30]</sup> and; (c) Al-Ti-B system as presented by Witusiewicz et al.<sup>[41]</sup>

have become the standard for this system.<sup>[30]</sup> For simplicity, this study considers  $TiC_y$  to be stoichiometric  $TiC$  (see below) and is represented as such in the ternary phase diagram.

**1.3.3 Ti-B-C System.** There are no ternary compounds in this system. The phase relations between the binary phases have been well established.<sup>[34]</sup>

**1.3.4 Al-Ti-B System.** No ternary phases exist in this system either. Isothermal sections at 800, 1000, 1350, and 1550 °C exist and show a dependence of the equilibrium phase relations on temperature. The most notable change in equilibrium relations is that  $TiB_2$  and  $AlB_2$  are in equilibrium at 800 °C, but not at, or above, 1000 °C.<sup>[39]</sup> This is due to the thermodynamic instability of  $AlB_2$  due to the aforementioned decomposition reaction (Eq 1), though it should be noted that the transformation rate is slow.<sup>[26,40]</sup> The computationally determined Al-Ti-B isotherms generated by Witusiewicz et al.<sup>[41]</sup> have been confirmed by experimental results and provide reliable equilibrium phase relations at 1000 °C (Fig. 1c). Again, non-stoichiometric phases are represented as point compounds.

The aim of this work was to investigate phase equilibria in the Al-Ti-B-C quaternary system at processing temperatures and compositions typical for the fabrication of Al matrix composites, i.e., near the Al corner and in the 900-1050 °C temperature range. To reach that goal, x-ray diffraction (XRD) and a scanning electron microscope (SEM) were used to characterize the reaction phases produced when  $Ti_2AlC/B_4C$  porous preforms were infiltrated by molten Al.

## 2. Experimental Procedures

### 2.1 Materials

Pure Al (99+%, Alfa Aesar, Ward Hill, MA) bar stock and  $B_4C$  powder (99+%, Alfa Aesar, Ward Hill, MA) with an average particle size  $< 10 \mu m$  was used for this work. Commercial -325 mesh  $Ti_2AlC$  powders were obtained (Kanthal, Sweden). It is worth noting here that  $Ti_3AlC_2$  is an impurity phase found in these powders ( $\approx 17$  wt.% from Rietveld analysis).

Two composites were fabricated starting with Al,  $Ti_2AlC$ , and  $B_4C$ . The first composite, henceforth referred to as BR, was more boron rich, having the Al:Ti:B:C molar ratio, calculated from Rietveld analysis of equilibrated microstructures (see below), of 3.3:1.1:2.5:0.5. The second composite, henceforth referred to as TiR, was more Ti-rich and the Al:Ti:B:C molar ratios in this case—again calculated from Rietveld analysis—were 3.4:1.1:1.3:0.7.

## 2.2 Processing

**2.2.1 Preparation of Carbide Preforms.** The  $\text{Ti}_2\text{AlC}/\text{B}_4\text{C}$  powders were mixed in the molar ratios of 4.5:5 and 7:4 for the BR and TiR composites, respectively. These ratios correspond to roughly 50/50 and 75/25 vol.% ratios of  $\text{Ti}_2\text{AlC}/\text{B}_4\text{C}$  for the BR and TiR composites, respectively. The mixed powders were ball milled for 24 h with yttria stabilized zirconia grinding media, cold pressed in a steel mold—to a load corresponding to a stress of 50 MPa—to form rectangular (BR =  $6.1 \times 12.7 \times 69.4 \text{ mm}^3$  and TiR =  $8.1 \times 12.8 \times 69.3 \text{ mm}^3$ )  $\approx 47$  vol.% porous preforms. The preform densities were 1.76 and 1.98  $\text{g}/\text{cm}^3$  for the BR and TiR preforms, respectively. Component densities were assumed to be 4.11  $\text{g}/\text{cm}^3$  for  $\text{Ti}_2\text{AlC}$  and 2.52  $\text{g}/\text{cm}^3$  for  $\text{B}_4\text{C}$ . No impurities or non-stoichiometry were considered.

**2.2.2 Pressureless Melt Infiltration.** The preforms were placed in alumina crucibles (AdValue Technology, Tucson, AZ), which were lined with graphite foil to avoid reactions with the crucible. Appropriately sized pieces of Al were placed on top of the preform and the assembly was placed in an alumina tube furnace and heated at a rate of 10  $^\circ\text{C}/\text{min}$  to 900, 950, 1000, or 1050  $^\circ\text{C}$  and allowed to soak for 0.5 h before furnace cooling to room temperature, RT. All experiments were carried out under flowing argon, Ar, gas at atmospheric pressure. The samples infiltrated at 1000  $^\circ\text{C}$  were cut in half and one half was further annealed at 1000  $^\circ\text{C}$  for 10 h, again under flowing Ar.

## 2.3 Microstructure Characterization

After cross-sectioning, mounting, and polishing (1200 grit) the microstructures were imaged using a SEM (Zeiss Supra 50VP, Germany) equipped with an energy-dispersive spectroscope (EDS) (Oxford Inca X-Sight, Oxfordshire, UK). Image analysis was undertaken using MATLAB (The MathWorks, Inc., Natick, MA) on select backscatter electron SEM micrographs to estimate the volume fractions of the various phases.

Powders for XRD were obtained by drilling the composites with a carbide drill bit and analyzed using a x-ray diffractometer (Rikagu Smartlab, Japan). The angular step was set to 0.02 $^\circ$  over the  $2\theta = 5^\circ$ –80 $^\circ$  range, with a hold time of 0.5 and 2 s for 0.5 h infiltration and equilibration experiments, respectively. Scans were made through a 10 $\times$ 10 mm<sup>2</sup> window slit using Cu K $\alpha$  radiation (40 KV and 30 mA).

To verify the presence of  $\text{Al}_4\text{C}_3$ , additional careful powder XRD was conducted on the equilibrium samples of both compositions. Powder was prepared immediately prior to running the XRD patterns. An angular step of 0.02 $^\circ$  was set over the range  $2\theta = 30^\circ$ –33 $^\circ$  and 39.5 $^\circ$ –40.5 $^\circ$ , with a hold time of 7 s. The slit and radiation conditions were the same as above. The hold time was extended here to enhance the intensity of the various peaks.

Rietveld refinements of the XRD patterns of the equilibrated samples were conducted using *FullProf*.<sup>[42]</sup> Refined parameters were: six background parameters, lattice parameters of all phases, scale factors from which relative

phase fractions are evaluated, and  $X$  profile parameters for peak width.

## 3. Results

### 3.1 Equilibrated Samples

**3.1.1 Phase Equilibria.** Table 1 summarizes the results obtained in this work. Phase identification, from both XRD and SEM/EDS, revealed that neither  $\text{Ti}_2\text{AlC}$  nor  $\text{B}_4\text{C}$  was an equilibrium phase in either composite. After annealing at 1000  $^\circ\text{C}$  for 10 h, the phases present in the BR sample, as determined by XRD were: Al,  $\text{TiB}_2$ ,  $\text{Al}_4\text{C}_3$  and  $\text{Al}_3\text{BC}$  (Table 1; Fig. 2a); those present in the TiR sample were: Al,  $\text{TiB}_2$ ,  $\text{Al}_4\text{C}_3$ , and TiC (Table 1; Fig. 2b). In other words, Al,  $\text{TiB}_2$ , and  $\text{Al}_4\text{C}_3$  were equilibrium phases in both compositions. For the BR and TiR compositions, all diffraction peaks were accounted for, with Rietveld  $\chi^2$  values of 5.12 and 8.60, respectively.

The presence of  $\text{Al}_4\text{C}_3$  was not apparent at first. The low intensity of its diffraction peaks were difficult to distinguish from background noise acquired with 0.5 s hold times. Further XRD patterns of the equilibration samples, using a 2 s hold time (Fig. 2), provided confidence that  $\text{Al}_4\text{C}_3$  diffraction peaks were present. XRD patterns obtained with a hold time of 7 s, however, left no doubt as to the presence of this phase in the equilibrated samples (insets of Fig. 2).

**3.1.2 Microstructures of Samples.** The BR composite soaked at 1000  $^\circ\text{C}$  for 0.5 h seemed to exhibit a homogeneous microstructure, with relatively large  $\text{B}_4\text{C}$  grains (black areas in Fig. 3a) remaining. Image analysis estimated the unreacted  $\text{B}_4\text{C}$  fraction to be  $\approx 2.5$  vol.%. In addition to the equilibrium phases present in the BR composite, traces of  $\text{AlB}_2$  and TiC could be found within the Al matrix when viewed at high magnification in the SEM (Fig. 3b). When the microstructure of the sample infiltrated for 0.5 h at 1000  $^\circ\text{C}$  was compared with the one held for 10 h at the same temperature (compare Fig. 3a, c, respectively) it is clear that:

(i) Al-containing phases, primarily  $\text{Al}_3\text{BC}$ , replace  $\text{B}_4\text{C}$ ; (ii) the volume fraction of the Al/ $\text{TiB}_2$  regions (light grey contrast in Fig. 3a, c) increased at the expense of the Al/ $\text{Al}_3\text{BC}$  regions (mid grey contrast) as the system tended towards equilibrium. The  $\text{B}_4\text{C}$  volume fraction after the 10 h anneal was estimated to be <1 vol.%. Aside from the remaining  $\text{B}_4\text{C}$ , no other non-equilibrium phases could be identified from microscopy (Fig. 3d); (iii) the  $\text{TiB}_2$  grains in the Al matrix were observed to notably coarsen with the prolonged annealing, growing from an estimated average diameter of <200 to >500 nm (Fig. 3b, d); (iv)  $\text{TiB}_2$  grains are found in the Al matrix, but not in the same regions as the  $\text{Al}_4\text{C}_3$  or  $\text{Al}_3\text{BC}$  phases (Fig. 3d).

The presence of  $\text{Al}_4\text{C}_3$  was not directly observed in the SEM in any of the investigated samples. However, since  $\text{Al}_4\text{C}_3$  is hygroscopic and dissolves in water at room temperature<sup>[43]</sup> it is reasonable to assume that it dissolved during the water-based polishing procedure. Note that EDS analysis of cross-sectional SEM micrographs clearly show that some Al-rich regions were comprised of pure Al; others

**Table 1** Observed phases from each experiment are reported with their relative increase or decrease in amount noted, if applicable, and calculated volume fractions, if available

Soaking time	Composite	Temperature (°C)	Major phases				Minor phases			
			(Relative increase ↑/Decrease ↓)				(Relative increase ↑/Decrease ↓)			
Results from image analysis										
0.5 h	BR	900	Al	TiB <sub>2</sub>	Al <sub>3</sub> BC	Al <sub>4</sub> C <sub>3</sub>	B <sub>4</sub> C (5.4 vol.%)	TiC	AlB <sub>2</sub>	
		950	Al (↓)	TiB <sub>2</sub> (↑)	Al <sub>3</sub> BC (↑)	Al <sub>4</sub> C <sub>3</sub> (↑)	B <sub>4</sub> C (5.1 vol.%)	TiC (↓)	AlB <sub>2</sub> (↓)	
		1050	Al (↓)	TiB <sub>2</sub> (↑)	Al <sub>3</sub> BC (↑)	Al <sub>4</sub> C <sub>3</sub> (↑)	B <sub>4</sub> C (2.1 vol.%)	TiC (↓)	AlB <sub>2</sub> (↓)	
	TiR	900	Al	TiAl <sub>3</sub>	TiC	TiB <sub>2</sub>	Al <sub>4</sub> C <sub>3</sub>	B <sub>4</sub> C (9.6 vol.%)	Ti <sub>3</sub> AlC <sub>2</sub> (5.3 vol.%)	
		950	Al (↑)	Al <sub>3</sub> BC	TiB <sub>2</sub> (↑)	TiC (↑)	Al <sub>4</sub> C <sub>3</sub> (↑)	B <sub>4</sub> C (4.7 vol.%)	TiAl <sub>3</sub> (↓)	
		1050	Al (↑)	TiB <sub>2</sub> (↑)	TiC (↑)		Al <sub>4</sub> C <sub>3</sub> (↑)	B <sub>4</sub> C (<1 vol.%)		
0.5 h	BR	1000	Al	TiB <sub>2</sub>	Al <sub>3</sub> BC	Al <sub>4</sub> C <sub>3</sub>	B <sub>4</sub> C (2.5 vol.%)	TiC	AlB <sub>2</sub>	
10 h		1000	Al	TiB <sub>2</sub>	Al <sub>3</sub> BC	Al <sub>4</sub> C <sub>3</sub>	B <sub>4</sub> C (<1 vol.%)			
0.5 h	TiR	1000	Al	TiB <sub>2</sub>	TiC	Al <sub>4</sub> C <sub>3</sub>	B <sub>4</sub> C (<1 vol.%)			
10 h		1000	Al	TiB <sub>2</sub>	TiC	Al <sub>4</sub> C <sub>3</sub>	B <sub>4</sub> C (<1 vol.%)			
Results from Rietveld analysis										
10 h	BR	1000	Al	TiB <sub>2</sub>	Al <sub>3</sub> BC	Al <sub>4</sub> C <sub>3</sub>				
			32.8 wt.%	44.6 wt.%	15.9 wt.%	7.1 wt.%				
TiR	1000	Al	TiB <sub>2</sub>	TiC	Al <sub>4</sub> C <sub>3</sub>					
		49.8 wt.%	26.2 wt.%	17.4 wt.%	6.6 wt.%					

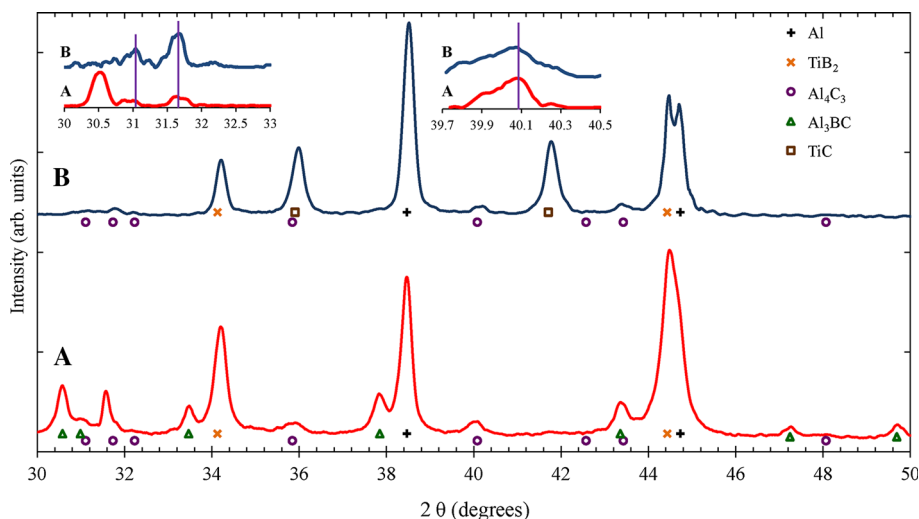


**Fig. 2** Typical XRD patterns for, (a) BR and, (b) TiR composites after equilibrating at 1000 °C for 10 h under flowing Ar. In both systems, Al, TiB<sub>2</sub>, and Al<sub>4</sub>C<sub>3</sub> were equilibrium phases. The presence of Al<sub>4</sub>C<sub>3</sub> in both composites was confirmed by additional investigations (marked by vertical lines in the insets)

were found to contain substantial amounts of C with Al/C ratios that varied between 1.0 and 1.9. It is hereby acknowledged that there are several explanations for why C may be detected in some Al regions and not others, including, the presence of C-containing phases below the surface, but within the excitation volume of the EDS. Nevertheless, since Al<sub>4</sub>C<sub>3</sub> peaks were observed—and twice

confirmed—in the XRD patterns (insets in Fig. 2), there is no doubt that it exists in the microstructures. Another possibility is that the Al<sub>4</sub>C<sub>3</sub> phase for some reason dissociated into C-rich Al regions. Therefore, the C-rich Al regions are tentatively labeled as Al<sub>4</sub>C<sub>3</sub> in the micrographs. These comments notwithstanding, more work is needed to understand what happens to the Al<sub>4</sub>C<sub>3</sub> phase.

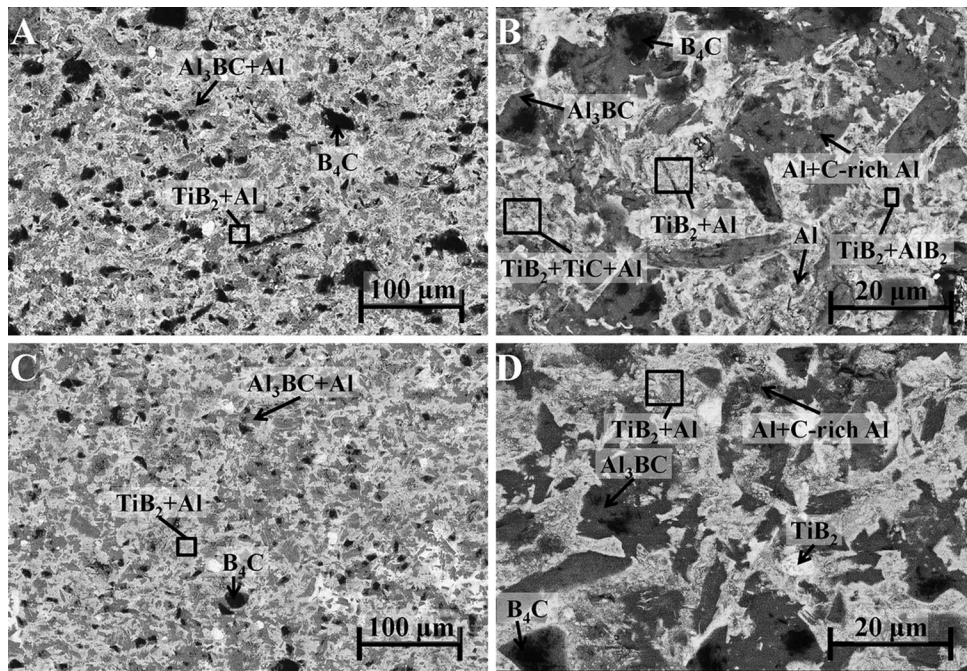


**Fig. 3** Backscattered electrons SEM images of BR samples fabricated at 1000 °C. (a) Low magnification image of sample annealed for 0.5 h. Large unreacted  $B_4C$  grains (black) can be found amongst  $Al_3BC/Al$  (mid grey) and  $TiB_2/Al$  (light grey) regions. (b) Higher magnification image of (a) demonstrating the presence of two distinct regions. Note the small grains of  $TiB_2$  dispersed in Al, whereas  $Al_3BC$  grains tend to be much larger. (c) Low magnification image of sample annealed for 10 h. The decreased fraction of remaining  $B_4C$  grains (black) corresponds to an increase in the  $TiB_2/Al$  (light grey) regions. (d) Higher magnification image of (c) demonstrating the increased grain size of  $TiB_2$  grains in the Al matrix

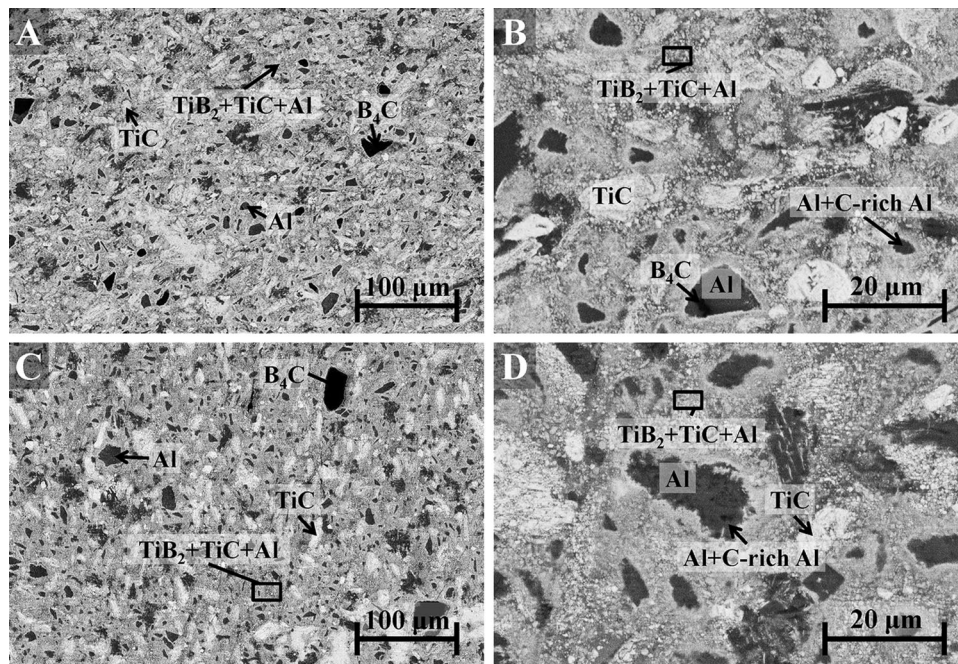


**Fig. 4** Backscattered electrons SEM images of TiR sample annealed at 1000 °C. (a) Low magnification image demonstrating homogeneous microstructure after 0.5 h anneal time. Some grains of  $B_4C$  (black) can be found remaining. (b) Higher magnification image of (a) showing small  $TiC/TiB_2$  grains dispersed in the Al matrix. (c) Low magnification image of sample annealed for 10 h. (d) Higher magnification image of (c) demonstrating similar grain dispersion to (b)



A relatively homogeneous microstructure was also obtained for the TiR composite after soaking at 1000 °C for 0.5 h (Fig. 4a). Larger TiC grains were found surrounded by an Al matrix; small grains of TiB<sub>2</sub> and TiC were distributed throughout. With the exception of a few remaining B<sub>4</sub>C grains—accounting for approximately <1 vol.%—and the possible formation of Al<sub>3</sub>BC at the B<sub>4</sub>C/Al interfaces, the only phases identified were—Al, TiC, TiB<sub>2</sub> and C-rich Al areas (Fig. 4b). After annealing for 10 h, the microstructure remained largely unchanged (Fig. 4c). Trace amounts of B<sub>4</sub>C (<0.5 vol.%) were still present after the 10 h anneal (Fig. 4d). In this case, no significant grain coarsening was observed for the small (<1 μm) TiB<sub>2</sub> and TiC grains.

### 3.2 Samples Melt Infiltrated for 0.5 h

**3.2.1 XRD of Reaction Products.** Complete infiltration of both BR and TiR composite preforms was observed after 0.5 h over the 900-1050 °C temperature range. The most

intense XRD peaks corresponded to those belonging to Al, Al<sub>3</sub>BC and TiB<sub>2</sub> (Fig. 5). Peaks associated with Al<sub>4</sub>C<sub>3</sub>, were weak at all temperatures (Fig. 5). At 900 °C (Fig. 5a) peaks belonging to B<sub>4</sub>C at  $2\theta = 34.96^\circ$ , were observed. At 950 °C and higher temperatures, no B<sub>4</sub>C peaks were observed (Fig. 5b, c).

Additionally, the TiC peak intensities decreased with increasing infiltration temperatures (see peak at  $2\theta = 41.71^\circ$  in Fig. 5). As AlB<sub>2</sub> shares its dominant XRD peaks with other phases, its presence was better ascertained by microscopy. The shoulder in the TiB<sub>2</sub> peak, at  $2\theta = 34.41^\circ$ , may be the best diffraction evidence that the quantity of AlB<sub>2</sub> decreases with MI temperature, as this shoulder is no longer observed after MI at 1050 °C (Fig. 5c).

For the TiR composite fabricated at 900 °C (Fig. 6a), prominent XRD peaks for Ti<sub>3</sub>AlC<sub>2</sub> were found along with those for TiAl<sub>3</sub>, TiC, and Al. However, by 950 °C peaks associated with Ti<sub>3</sub>AlC<sub>2</sub> disappeared, and the peak

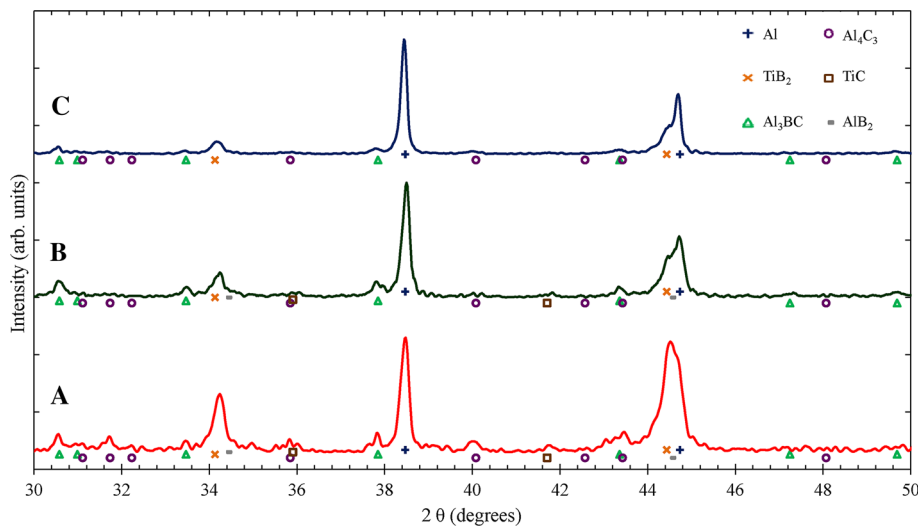


**Fig. 5** X-ray diffraction patterns for BR samples infiltrated and held at (a) 900, (b) 950 and, (c) 1050 °C for 0.5 h

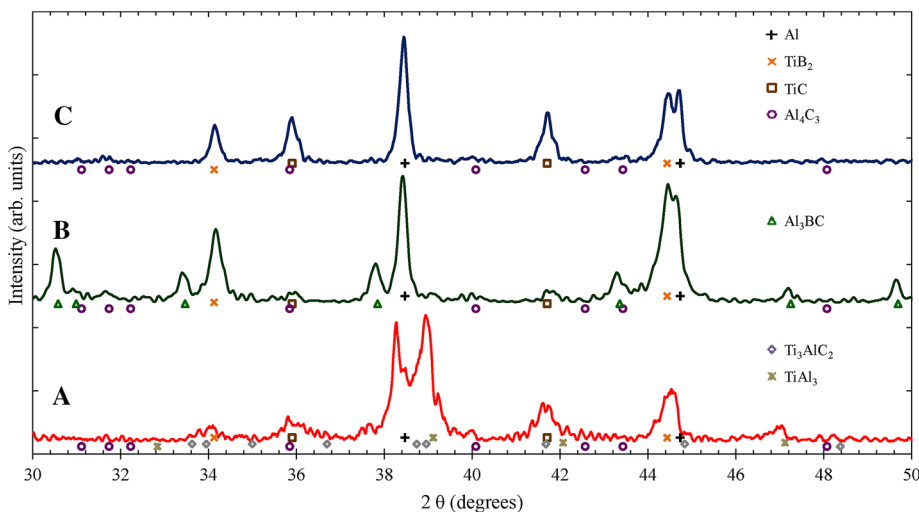


**Fig. 6** X-ray diffraction patterns for TiR samples infiltrated and held at (a) 900, (b) 950 and, (c) 1050 °C for 0.5 h

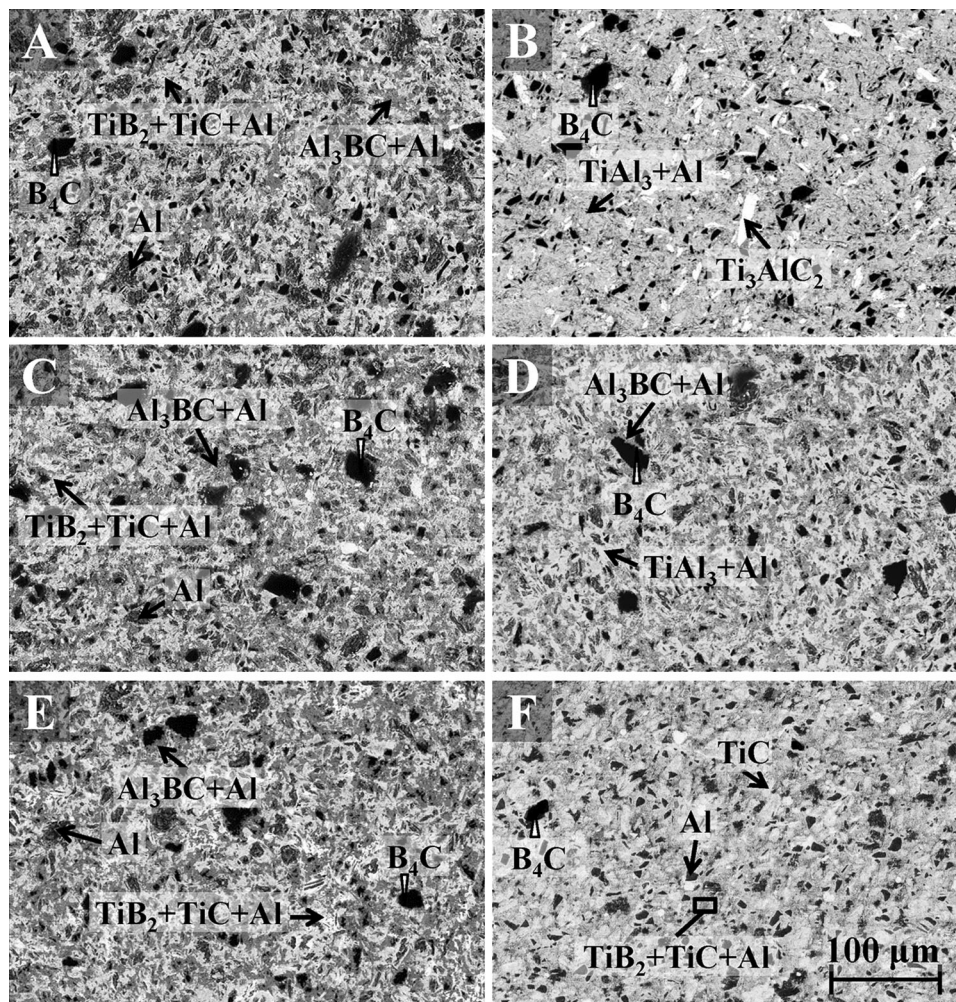


**Fig. 7** Backscattered electrons SEM images of BR (left) and TiR (right) infiltration experiments annealed for 0.5 h. (a) BR sample processed at 900 °C demonstrating the highest fraction of unreacted  $B_4C$  (black). (b) TiR sample processed at 900 °C demonstrating the presence of  $Ti_3AlC_2$ , with needle-like grain morphology, dispersed in a  $TiAl_3/Al$  matrix. (c) BR sample processed at 950 °C. (d) TiR sample processed at 950 °C.  $Ti_3AlC_2$  disappears and  $Al_3BC$  appears as  $B_4C$  and  $TiAl_3$  are consumed. (e) BR sample processed at 1050 °C demonstrating no distinguishable microstructural changes from A. (f) TiR sample processed at 1050 °C demonstrating a change in microstructure that is similar to the equilibrated sample (Fig. 4c). Scale bar applies to all panels

intensities associated with  $TiAl_3$  were significantly decreased, while those of  $TiB_2$  and  $Al_3BC$  were seen to emerge (Fig. 6b). At 1050 °C, the XRD patterns (Fig. 6c) clearly showed that the phases present were the same as those observed after 10 h at 1000 °C (Fig. 2b), viz. Al,  $TiB_2$ , TiC and  $Al_4C_3$ .

**3.2.2 Microstructures of Samples.** Not surprisingly, the BR composite sample fabricated at 900 °C was the farthest from equilibrium, since it contained the largest content of the non-equilibrium phases, TiC and  $AlB_2$  and  $B_4C$  (Table 1). Aside from the presence of these non-equilibrium phases, the BR composites infiltrated at 900 °C (Fig. 7a), 950 °C (Fig. 7c), and 1050 °C (Fig. 7e) were relatively homogeneous, with two distinct regions: The first consisted of  $Al_3BC$  and the second  $TiB_2/TiC$  both in Al matrices (Fig. 7a, c, e). The differences between the two regions are best seen at higher magnification of the sample infiltrated at

1050 °C (Fig. 8). Note that C-rich Al regions were also found alongside  $Al_3BC$  in the Al matrix, but not in regions containing the Ti phases. The  $TiB_2/TiC$  regions also contained  $AlB_2$  (Fig. 8). Because of their small grain size (<1 μm diameter) it was not possible to estimate the volume fractions of these phases from image analysis. Note that, for similar reasons, it was difficult to precisely identify the composition of individual grains from EDS.

After MI at 900 °C, needle-like grains of  $Ti_3AlC_2$  could be seen dispersed throughout an  $Al/TiAl_3$  matrix (Fig. 7b). From image analysis, the  $Ti_3AlC_2$  volume fraction was estimated to be ≈5.3 vol.%. This infiltration temperature also resulted in the largest volume fraction of unreacted  $B_4C$  (Table 1). Higher magnification SEM micrographs revealed that this composite was primarily (≈85 vol.%)  $TiAl_3$ , in equilibrium with Al and that little reaction had occurred with the  $B_4C$  phase (Fig. 9a).

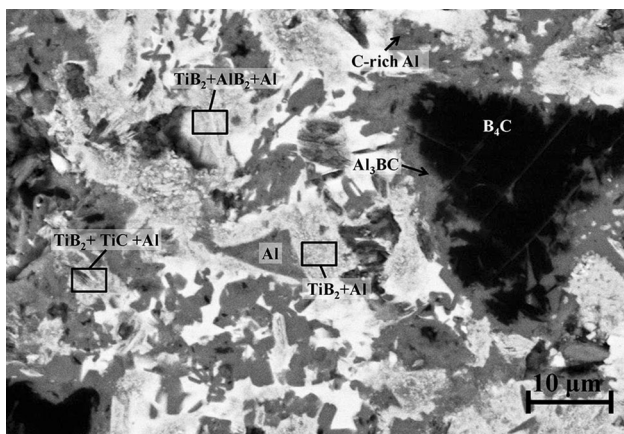


**Fig. 8** Backscattered electrons SEM image of BR sample infiltrated and held at 1050 °C for 0.5 h

Raising the infiltration temperature to 950 °C resulted in the disappearance of the  $\text{Ti}_3\text{AlC}_2$  phase from both the XRD and SEM results (Fig. 6b, 7d). The microstructure at this temperature consisted of fine grains of  $\text{TiB}_2$  and  $\text{TiC}$  contained in an  $\text{Al}/\text{TiAl}_3$  matrix, with some unreacted  $\text{B}_4\text{C}$  grains remaining (Fig. 7d). The latter were surrounded by  $\text{Al}_3\text{BC}$ . The C-rich Al-containing regions were not found in regions of Ti-containing phases, but were only found in the vicinity of the Al and  $\text{Al}_3\text{BC}$  phases (Fig. 9b). After the 1050 °C infiltration, there was no trace of  $\text{TiAl}_3$ ; the only phases remaining were  $\text{TiC}$ ,  $\text{TiB}_2$ , Al and C-rich Al-containing regions, with trace amounts of  $\text{B}_4\text{C}$  (Fig. 7f).

In contrast to the microstructures seen after MI at 900 °C (Fig. 9a) and 950 °C (Fig. 9b), the ones MI at 1000 °C (Fig. 4b) and 1050 °C (Fig. 9c) showed regions with evenly dispersed grains of  $\text{TiC}$  and  $\text{TiB}_2$  in an Al matrix. The ternary  $\text{Al}_3\text{BC}$  was not found above 950 °C and the large  $\text{B}_4\text{C}$  grains were replaced by some C-containing Al matrix regions, surrounded by a  $\approx 0.5 \mu\text{m}$  wide Ti-rich layer (Fig. 9c).

## 4. Discussion

### 4.1 Equilibrium Tetrahedra

**4.1.1 B-Rich Composite.** Based on the totality of our XRD and SEM results on the equilibrated BR composition it is reasonable to conclude that the 4 apexes of this equilibrium tetrahedron are: Al,  $\text{Al}_3\text{BC}$ ,  $\text{TiB}_2$ , and  $\text{Al}_4\text{C}_3$  (pink tetrahedron in Fig. 10a, c and Supplementary Information). The starting molar composition (blue circle in Fig. 10a), clearly falls within this equilibrium tetrahedron. Note that the size of this tetrahedron is relatively small—only occupying 2.86 vol.% of the phase diagram.

To examine the robustness of our conclusions, the position of the initial composition was re-calculated assuming that the stoichiometry of  $\text{B}_4\text{C}$  to be  $\text{B}_4\text{C}_{0.5}$ , with all else remaining the same. When plotted, this composition point shifted by a negligible amount. We also carried out a

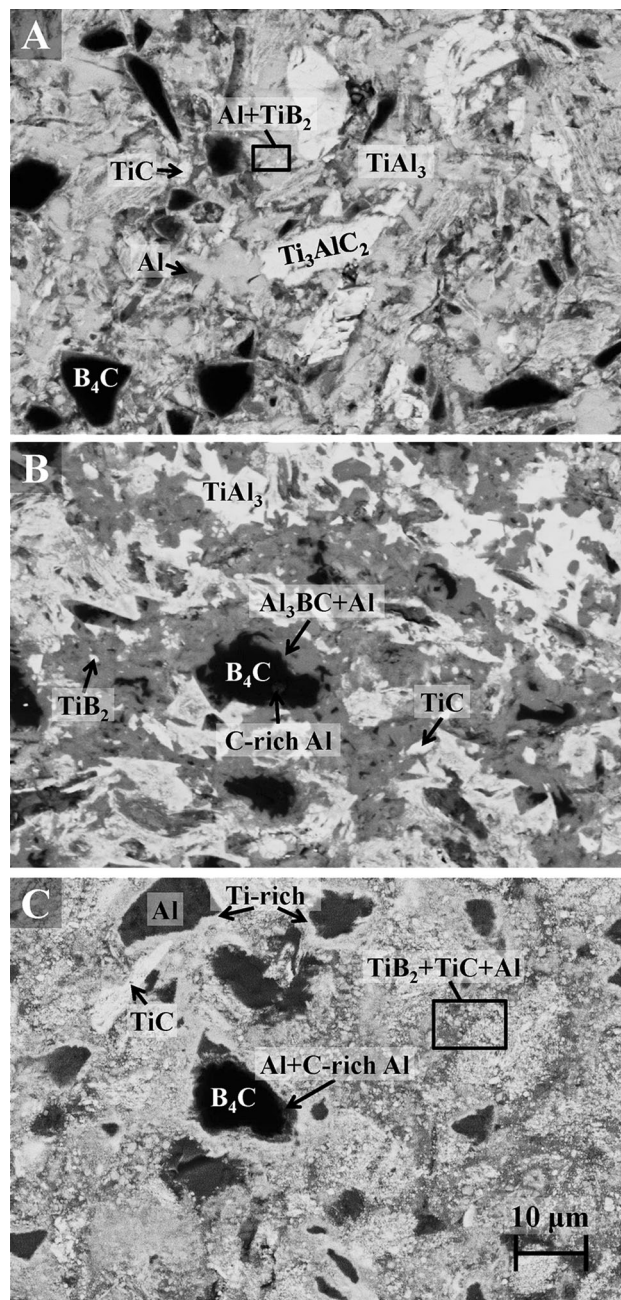


**Fig. 9** Backscattered electrons SEM image of Ti-rich infiltration experiment at (a) 900 °C, (b) 950 °C, and (c) 1050 °C for 0.5 h. Scale bar applies to all panels

calculation incorporating the presence of 20 wt.%  $\text{Ti}_3\text{AlC}_2$  in the starting composition. In that case the initial Al:Ti:B:C molar ratio is 3.8:0.9:3.0:1.2. The resulting location point was nearly indiscernible from the location of the blue circle shown in Fig. 10(a).

Based on these findings, it can be concluded that neither the  $\text{B}_4\text{C}$  stoichiometry nor the presence of  $\approx 20$  wt.%  $\text{Ti}_3\text{AlC}_2$  in the initial powder affects the location of the initial composition in the conjectured equilibrium tetrahedron.

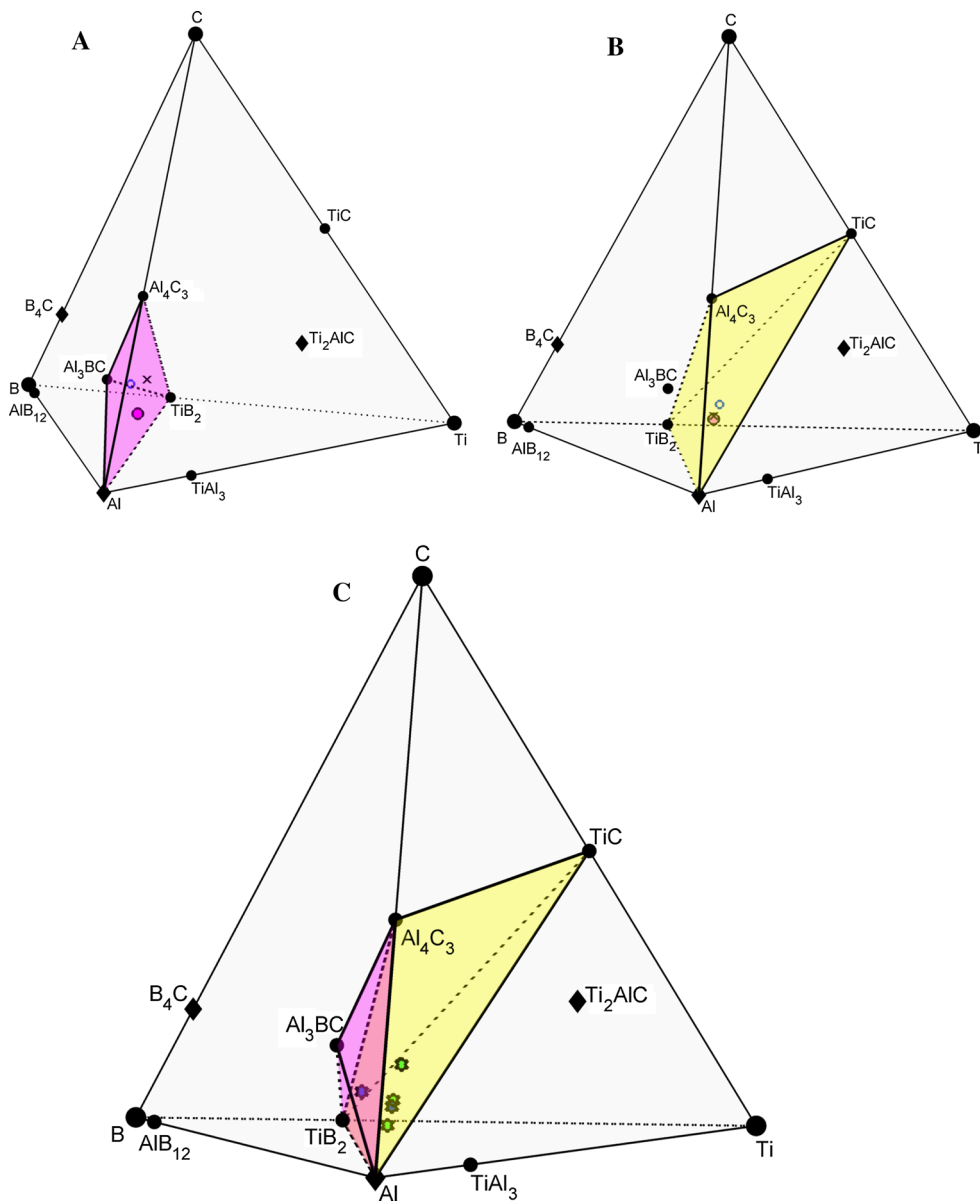


**Fig. 10** Equilibrium tetrahedron as determined from, (a) B-rich composition. Open blue circle represents the starting composition as calculated from starting powder weights, black x represents the composition as determined from the left hand side of Eq. 7; pink point represents the final molar composition as determined from Rietveld analysis of equilibrated samples. (b) Ti-rich composition. Open blue circle represents the starting composition as calculated from starting powder weights, black x represents the composition as determined from the left hand side of Eq. 14; pink point represents the final molar composition as determined from Rietveld analysis of equilibrated samples. (c) Constituent Al-Ti-B-C phase diagram at 1000 °C. Green points represent 10, 40, and 60 wt.% Al compositions from Zou et al.<sup>[24]</sup> and blue points are the nominal compositions reported by Zhang et al.<sup>[48]</sup> (Color figure online)

Based on the Rietveld refinements, the final Al:Ti:B:C molar ratio was calculated to be 3.8:1.3:2.9:0.6 (pink point in Fig. 10a) with corresponding high volume fractions of Al and TiB<sub>2</sub> (Table 1). The discrepancy between the initial (3.8:0.9:3.0:1.2) and final molar compositions in this system is discussed below. However, as both compositions lie within the *same* equilibrium tetrahedron, this discrepancy in no way affects the conclusions of this study.

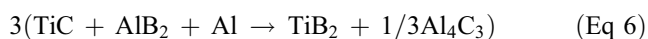
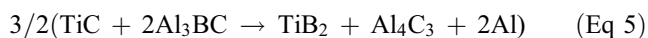
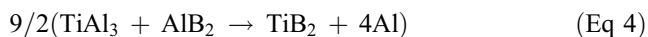
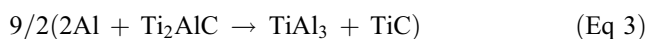
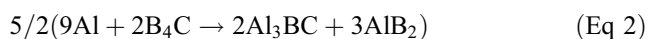
**4.1.2 Ti-Rich Composite.** Based on the totality of our XRD and SEM results on the equilibrated TiR composition it is reasonable to conclude that the 4 apexes of this equilibrium tetrahedron are: Al, TiB<sub>2</sub>, Al<sub>4</sub>C<sub>3</sub>, and TiC (tan tetrahedron in Fig. 10b-c and Supplementary Information). The latter occupies a larger volume of the phase diagram (14.29 vol.%) than the B-rich composition and was also found to be unaffected by non-stoichiometries in the B<sub>4</sub>C and/or the presence of Ti<sub>3</sub>AlC<sub>2</sub>. In this case, the starting

composition (blue circle in Fig. 10b) was in excellent agreement with the composition calculated from Rietveld refinement of the XRD results (pink point in Fig. 10b) after equilibration, with both compositions well within the boundaries of the equilibrium tetrahedron.

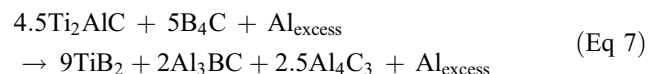
**4.1.3 Constituent Phase Diagram at 1000 °C.** An interactive quaternary phase diagram can be found in Supplementary Materials. Note that this phase diagram assumes all phases to be line compounds (Fig. 10c). That this is an oversimplification is obvious for the simple reason that TiC exists over a wide Ti:C molar ratio. However, since this is the first report of this quaternary phase diagram, and for the sake of simplicity, we chose to assume TiC and all other compounds to be line compounds. Understanding how the non-stoichiometry of TiC affects the diagram is important and should be mapped out, but is beyond the scope of this work.

## 4.2 Reaction Mechanisms

**4.2.1 B-Rich Composites.** Based on the results summarized in Table 1, together with the reaction-path-superimposed quaternary phase diagram (Supplementary 1)—where dashed lines represent reacting phases, solid lines represent reaction products, and bold lines outline the equilibrium phase relations—the following reactions are surmised to occur in the BR composition:



for the overall reaction:

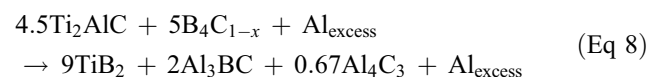


Upon wetting of the preform by molten Al, the initial reactions would be between Al/B<sub>4</sub>C and Al/Ti<sub>2</sub>AlC according to Eq 2 and 3, respectively. AlB<sub>2</sub> and Al<sub>3</sub>BC are in equilibrium below the peritectic transformation temperature of AlB<sub>2</sub>, and B<sub>4</sub>C has been reported to react with Al to form these products in various experiments.<sup>[40,44,45]</sup> Both of these phases were observed herein. The reaction of Ti<sub>2</sub>AlC with Al (Eq 3) at the investigated temperatures is in agreement with the surmised reaction path of Ti<sub>3</sub>AlC<sub>2</sub> with Al above 900 °C.<sup>[12,20]</sup>

Reaction 3 is also to be expected from an inspection of the ternary phase diagram (Fig. 1b) as the TiC/TiAl<sub>3</sub> equilibrium line must be crossed in reacting Al with the Ti<sub>2</sub>AlC (labeled 'H' in Fig. 1b). While TiAl<sub>3</sub> was not observed in this system, its production by this reaction is presented clearly in the TiR composite fabricated at 900 °C (see below). Of the four phases produced by these two

reactions (Eq 2 and 3) only Al<sub>3</sub>BC is an equilibrium phase, indicating that the transient phases—AlB<sub>2</sub>, TiAl<sub>3</sub>, and TiC—must at some point react to form equilibrium phases (Eq 4 and 5). The formation of TiB<sub>2</sub> by the reaction of TiAl<sub>3</sub> with AlB<sub>2</sub> has been previously reported in Al matrix composites, though largely through aluminothermic reactions of KF based salts in an Al melt.<sup>[46,47]</sup> Additionally, thermodynamic calculations indicate that the reaction between TiC and AlB<sub>2</sub> (Eq 6) is favorable in high temperature Al melts.<sup>[5]</sup> Lastly, the reaction between TiC and Al<sub>3</sub>BC (Eq 5) was inferred by the necessity to balance the overall reaction (Eq 7) and has not been found in the literature. It is not unreasonable to speculate about the feasibility of this reaction as it keeps in line with the finding that TiC is not stable in some Al-B systems.<sup>[5]</sup> The continual consumption of TiC in Eq 5 and 6 is in agreement with the decreasing TiC peak intensities in the XRD spectra acquired for each infiltration temperature (Fig. 5).

Rietveld analysis of the equilibrium microstructure resulted in the overall reaction:



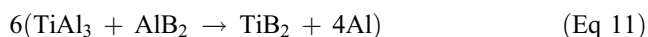
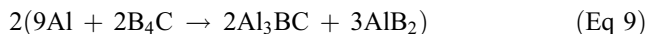
In general, the agreement between the surmised reaction (Eq 7) and reaction Eq 8 is excellent with the only difference being that the Rietveld calculations show less Al<sub>4</sub>C<sub>3</sub> than surmised. The cause of this may be rationalized in two ways: (i) some amount of Al<sub>4</sub>C<sub>3</sub> may have hydrolyzed and became amorphous prior to the collection of the XRD patterns, which would under represent the amount of Al<sub>4</sub>C<sub>3</sub> in the Rietveld calculations; and/or (ii) non-stoichiometric B<sub>4</sub>C and/or impurities in the starting powders may be responsible for the production of less Al<sub>4</sub>C<sub>3</sub>. As noted above, however, since the molar compositions of both the left and right sides of Eq 8 clearly fall within the *same* equilibrium tetrahedron (black X and pink point in Fig. 10a, respectively) the unbalanced equation has no effect on the results of this study. It may be for similar reasons that there is a disagreement between molar compositions from Rietveld calculations and the starting powder weights; however, as all molar compositions fall within the *same* equilibrium tetrahedron the results of this study are sound.

Examination of the BR microstructures at each infiltration temperature coincides with the proposed reaction path. No MAX phase is observed in this system, indicating that Eq 3 must occur rapidly after wetting of the preform. The reaction with B<sub>4</sub>C (Eq 2), however, continues even after equilibration for 10 h (Fig. 3c). It has been suggested that Al<sub>3</sub>BC forms a diffusion barrier and limits the rate at which the B<sub>4</sub>C grains are consumed by Al and also the rate at which boron diffuses into the matrix.<sup>[40]</sup> The results shown herein support this finding. As evidence for TiAl<sub>3</sub> was also unobserved by our XRD or SEM investigations, and since more AlB<sub>2</sub> is produced (Eq 2) than TiAl<sub>3</sub> is consumed (Eq 4) it is probable that this reaction also occurs rapidly following the production of AlB<sub>2</sub>. This also explains why AlB<sub>2</sub> could be found in some microstructures (Fig. 3b, 8), as the remaining AlB<sub>2</sub> is proposed to be consumed by TiC

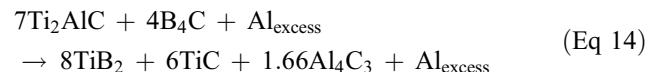
(Eq 5), presumably by a slower reaction since both of these phases were observed.

The higher magnification SEM micrographs of the sample fabricated at 1050 °C (Fig. 8) sheds more light on the reaction path: the un-reacted B<sub>4</sub>C is surrounded by an Al<sub>3</sub>BC layer (expected from Eq 2), AlB<sub>2</sub> is found in Ti-containing regions which is necessary if it is to react with TiC, and TiC was also found near the Al<sub>3</sub>BC phase, making it feasible that they could react to bring the system to equilibrium (Eq 6).

**4.2.2 Ti-Rich Composites.** In a similar fashion, the TiR composite system may be analyzed in light of the phase diagram developed herein. The suggested reaction path is:

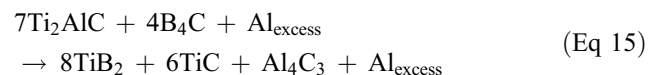


that sums to the overall reaction:



Since Eq 9-12 are identical to Eq 2-5, they will not be discussed further. However, in order to consume the remaining TiAl<sub>3</sub> and bring the system to equilibrium, Eq 13 is proposed. This reaction is expected from analysis of the Al-Ti-C ternary diagram (Fig. 1b) and has been reported to occur at temperatures above the melting point of Al.<sup>[31]</sup>

Rietveld analysis of the equilibrium microstructure translates to the following overall reaction:

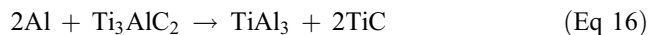


which, with the exception of Al<sub>4</sub>C<sub>3</sub>, is in excellent agreement with Eq 14. Here again the major discrepancy between two reactions is the lower amounts of Al<sub>4</sub>C<sub>3</sub> in the experimental results (Eq 15). Some of the reasons invoked to account for this deficiency in the BR composition may also apply here. This comment notwithstanding, more work is needed to further understand the discrepancy. However, since the molar compositions of both the left and right sides of Eq 15 fall within the *same* equilibrium tetrahedron (black X and pink point in Fig. 10b, respectively) the fact that Eq 15 is unbalanced has no effect on the quaternary diagram.

When the short time MI experiments for the TiR and BR compositions are compared, it becomes obvious that the sequence and rates of some of the reactions are notably different. For example, Ti<sub>2</sub>AlC was not observed in the TiR composition, but its reaction products (Eq 10) were seen in

the XRD patterns (Fig. 6a) and SEM micrographs (Fig. 9a). In contrast, the reaction products of B<sub>4</sub>C with Al, Al<sub>3</sub>BC and AlB<sub>2</sub> (Eq 9) phases were not observed after processing at 900 °C. This is clear evidence that Ti<sub>2</sub>AlC is less stable in excess Al than B<sub>4</sub>C. However, at 950 °C a notable shift in reaction products occurs. TiAl<sub>3</sub> is consumed and Al<sub>3</sub>BC is produced (Eq 9 and 11), likely the result of increased reactivity of B<sub>4</sub>C with Al (Eq 9) at the higher temperature. As with the BR system, this indicates that TiAl<sub>3</sub> is rapidly consumed upon the production of AlB<sub>2</sub> (Eq 11), as AlB<sub>2</sub> was not identified from XRD and the TiAl<sub>3</sub> peaks almost disappear (Fig. 6b). Al<sub>3</sub>BC is clearly a primary phase at 950 °C, which argues in favor of a slower reaction between TiC and Al<sub>3</sub>BC (Eq 12) than the rate at which Al<sub>3</sub>BC is produced. It may also be that Eq 12 is responsible for the change in microstructure between 950 and 1050 °C (Fig. 9b and c, respectively). The consumption of Al<sub>3</sub>BC (Eq 12) and remnant TiAl<sub>3</sub> (Eq 13) is necessary to bring the system to equilibrium.

**4.2.3 Reaction with Ti<sub>3</sub>AlC<sub>2</sub>.** The aforementioned reaction mechanisms coincide well with the observations in both BR and TiR systems. However, it is important to recognize the potential for other reactions to occur in this quaternary system. Ti<sub>3</sub>AlC<sub>2</sub> exists in the starting powder and was the only MAX phase to be observed in any of the composites (TiR at 900 °C, Fig. 7b); however, it was left out in the overall reaction scheme for simplicity. In both systems the likely reaction is:



as detailed in the literature.<sup>[12]</sup> However, given that the fraction of this phase in the starting powder is small, it is reasonable to assume that it would not have a significant impact on the overall reactions (Eq 8 or 14).

### 4.3 Comparison with Literature Results

The reaction products after melt infiltration at 1000 °C established in this work agree with the products reported by other researchers using similar compositions, but different reaction methods. For example, Zou et al.<sup>[24]</sup> produced TiC-TiB<sub>2</sub>-Al composites between 10 and 60 wt.% Al using self-propagating high-temperature synthesis. The maximum temperature of their reaction decreased from 2900 °C and approached the investigated temperature range of this work as the Al wt.% increased. Calculations show that their Al:Ti:B:C ratio ranges from 0.8:3.0:4.0:1.0 with 10 wt.% Al, to 11.1:3.0:4.0:1.0 with 60 wt.% Al. These compositions lie on the Al-TiB<sub>2</sub>-TiC face of the quaternary phase diagram (green points represent 10, 40, and 60 wt.% Al in Fig. 10c). In addition to these phases, they reported that Al<sub>4</sub>C<sub>3</sub> and TiAl<sub>3</sub> were also present in small amounts as a consequence of the fact that their system was not allowed to reach equilibrium.

Zhang et al.<sup>[48]</sup> utilized quick spontaneous infiltration to make composites from Ti-B<sub>4</sub>C-Al powder preforms (55-60% dense) dipped in molten Al at 920 °C. The nominal composition of two of their composites, with Al:Ti:B:C molar ratios of 6:3:6:1.5 and 6:3:4:1, fall on the Al-Al<sub>4</sub>C<sub>3</sub>-TiB<sub>2</sub> and Al-TiB<sub>2</sub>-TiC faces of the quaternary phase

diagram, respectively (blue points in Fig. 10c). In both composites, Al, TiB<sub>2</sub>, and TiC were the primary phases found. In the B-rich composite, some TiAl<sub>3</sub> was also detected. Neither Al<sub>4</sub>C<sub>3</sub> nor Al<sub>3</sub>BC was observed by XRD after infiltration or differential thermal analysis (DTA) of both composites. Consequently, they computationally determined that the likely equilibrium products of the more B-rich composite were Al<sub>3</sub>BC, TiB<sub>2</sub>, and TiAl<sub>3</sub>. Our findings show that TiAl<sub>3</sub> is not an equilibrium product of this composition.

However, the equilibrium phases present in the B-poor composition—Al, TiB<sub>2</sub>, and TiC—are in full agreement with our results.<sup>[48]</sup> Their conclusion that B<sub>4</sub>C is also in equilibrium with TiB<sub>2</sub> and TiC is at odds with our results. The most likely source of these discrepancies is the fact that Zhang et al.<sup>[48]</sup> did not allow their samples to reach equilibrium.

## 5. Summary

- The 1000 °C Al-Ti-B-C quaternary phase diagram in the Al-rich corner was determined. The final Al:Ti:B:C ratios in the equilibrated microstructures were 3.8:1.3:2.9:0.6 (B-rich) and 3.4:1.1:1.3:0.7 (Ti-rich).
- And while both compositions were located near the center of quaternary phase diagram, they belonged to two separate equilibrium tetrahedra. For the B-rich composition the equilibrium phases were Al, Al<sub>3</sub>BC, TiB<sub>2</sub> and Al<sub>4</sub>C<sub>3</sub>. In the Ti-rich case, the equilibrium phases were Al, TiC, TiB<sub>2</sub> and Al<sub>4</sub>C<sub>3</sub>.
- A reaction mechanism was proposed for both compositions to explain the observed reaction products after 0.5 h MI experiments and equilibrium conditions.

## Acknowledgments

This work was supported by the Army Research Office (W911NF-11-1-0525). Additionally, the authors would like to acknowledge Grady Bentzel, Darin Tallman, and Prof. El'ad Caspi for their assistance with Rietveld refinements.

## References

1. D.B. Miracle, Metal Matrix Composites—From Science to Technological Significance, *Compos. Sci. Technol.*, 2005, **65**, p 2526-2540
2. M.D. Sacks, H.W. Lee, and O.E. Rojas, Suspension Processing of Al<sub>2</sub>O<sub>3</sub>/SiC Whisker Composites, *J. Am. Ceram. Soc.*, 1988, **71**, p 370-379
3. B.S. Lee and S. Kang, Low-Temperature Processing of B<sub>4</sub>C–Al Composites Via Infiltration Technique, *Mater. Chem. Phys.*, 2001, **67**, p 249-255
4. A. Albiter, C.A. León, R.A.L. Drew, and E. Bedolla, Microstructure and Heat-Treatment Response of Al-2024/TiC Composites, *Mater. Sci. Eng. A*, 2000, **289**, p 109-115
5. H. Ding, X. Liu, and J. Nie, Study of Preparation of TiB<sub>2</sub> by TiC in Al Melts, *Mater. Charact.*, 2012, **63**, p 56-62
6. I. Ibrahim, F. Mohamed, and E. Lavernia, Particulate Reinforced Metal Matrix Composites—A Review, *J. Mater. Sci.*, 1991, **26**, p 1137-1156
7. Z. Zhang, K. Fortin, A. Charette, and X. Chen, Effect of Titanium on Microstructure and Fluidity of Al–B<sub>4</sub>C Composites, *J. Mater. Sci.*, 2011, **46**, p 3176-3185
8. J. Salem and E. Fuller, *Corrosion, Wear, Fatigue, and Reliability of Ceramics*, Wiley, New York, 2009
9. S. Amini, C. Ni, and M.W. Barsoum, Processing, Microstructural Characterization and Mechanical Properties of a Ti<sub>2</sub>AlC/Nanocrystalline Mg-Matrix Composite, *Compos. Sci. Technol.*, 2009, **69**, p 414-420
10. B. Anasori, S. Amini, V. Presser, and M.W. Barsoum, Nanocrystalline Mg-Matrix Composites with Ultrahigh Damping Properties, *Magnes. Technol.*, 2011, **2011**, p 463-468
11. B. Anasori, E.N. Caspi, and M.W. Barsoum, Fabrication and Mechanical Properties of Pressureless Melt Infiltrated Magnesium Alloy Composites Reinforced with TiC and Ti<sub>2</sub>AlC Particles, *Mater. Sci. Eng. A*, 2014, **618**, p 511-522
12. M.W. Barsoum, *MAX Phases: Properties of Machinable Ternary Carbides and Nitrides*, Wiley, New York, 2013
13. M.W. Barsoum and T. ElRaghy, Synthesis and Characterization of a Remarkable Ceramic: Ti<sub>3</sub>SiC<sub>2</sub>, *J. Am. Ceram. Soc.*, 1996, **79**, p 1953-1956
14. M.W. Barsoum, D. Brodtkin, and T. ElRaghy, Layered Machinable Ceramics for High Temperature Applications, *Scripta Mater.*, 1997, **36**, p 535-541
15. M.W. Barsoum, M.C. Flemings, E.J. Kramer, S. Mahajan, and P. Veyssiere, Physical Properties of the MAX Phases, *Encyclopedia of Materials Science and Technology*, K.H.J. Buschow, R.W. Cahn, and M.C. Flemings, Ed., Elsevier, Amsterdam, 2006,
16. D.J. Tallman, M. Naguib, B. Anasori, and M.W. Barsoum, Tensile Creep of Ti<sub>2</sub>AlC in Air in the Temperature Range 1000–1150 °C, *Scripta Mater.*, 2012, **66**, p 805-808
17. A. Kontsos, T. Loutas, V. Kostopoulos, K. Hazeli, B. Anasori, and M.W. Barsoum, Nanocrystalline Mg–MAX Composites: Mechanical Behavior Characterization Via Acoustic Emission Monitoring, *Acta Mater.*, 2011, **59**, p 5716-5727
18. M. Sundberg, G. Malmqvist, A. Magnusson and T. El-Raghy, Alumina Forming High Temperature Silicides and Carbides, *3rd Asian Meeting on Electroceramics (AMEC-3)*, Dec 7-11, 2003, Elsevier, UK, 2004, p. 1899-1904
19. B. Anasori, Fabrication and Mechanical Properties of Pressureless Melt Infiltrated Magnesium Alloy Composites Reinforced with TiC and Ti<sub>2</sub>AlC Particles, *Mater. Sci. Eng.*, 2014, **618**, p 511-522
20. W.J. Wang, V. Gauthier-Brunet, G.P. Bei, G. Laplanche, J. Bonneville, A. Joulain, and S. Dubois, Powder Metallurgy Processing and Compressive Properties of Ti<sub>3</sub>AlC<sub>2</sub>/Al Composites, *Mater. Sci. Eng. A*, 2011, **530**, p 168-173
21. L. Hu, A. Kothalkar, M. O'Neil, I. Karaman, and M. Radovic, Current-Activated, Pressure-Assisted Infiltration: A Novel, Versatile Route for Producing Interpenetrating Ceramic-Metal Composites, *Mater. Res. Lett.*, 2014, **2**, p 124-130
22. S.Y. Oh, J.A. Cornie, and K.C. Russell, Wetting of Ceramic Particulates with Liquid Aluminum Alloys: Part II. Study of Wettability, *Metall. Trans. A*, 1989, **20**, p 533-541
23. D.A. Weirauch, W.M. Balaba, and A.J. Perrotta, Kinetics of the Reactive Spreading of Molten Aluminum on Ceramic Surfaces, *J. Mater. Res.*, 1995, **10**, p 640-650
24. B. Zou, P. Shen, and Q. Jiang, Reaction Synthesis of TiC–TiB<sub>2</sub>/Al Composites from an Al–Ti–B<sub>4</sub>C System, *J. Mater. Sci.*, 2007, **42**, p 9927-9933

25. H. Okamoto, Al-B (Aluminum-Boron), *J. Phase Equilib. Diffus.*, 2006, **27**, p 195-196
26. A. Hall and J. Economy, The Al(L) + AlB<sub>12</sub> ↔ AlB<sub>2</sub> Peritectic Transformation and Its Role in the Formation of High Aspect Ratio AlB<sub>2</sub> Flakes, *JPE*, 2000, **21**, p 63-69
27. D. Mirković, J. Gröbner, R. Schmid-Fetzer, O. Fabrichnaya, and H.L. Lukas, Experimental Study and Thermodynamic Re-assessment of the Al-B System, *J. Alloy. Compd.*, 2004, **384**, p 168-174
28. C. Qiu and R. Metselaar, Solubility of Carbon in Liquid Al and Stability of Al<sub>4</sub>C<sub>3</sub>, *J. Alloy. Compd.*, 1994, **216**, p 55-60
29. T. Nukami and M.C. Flemings, In Situ Synthesis of TiC Particulate-Reinforced Aluminum Matrix Composites, *Metall Mater Trans A*, 1995, **26A**, p 1877-1884
30. M. Pietzka and J. Schuster, Summary of Constitutional Data on the Aluminum-Carbon-Titanium System, *JPE*, 1994, **15**, p 392-400
31. V. Raghavan, Al-C-Ti (Aluminum-Carbon-Titanium), *J. Phase Equilib. Diffus.*, 2006, **27**, p 148-149
32. L. Brewer and H. Haraldsen, The Thermodynamic Stability of Refractory Borides, *J. Electrochem. Soc.*, 1955, **102**, p 399-406
33. H. Okamoto, B-Ti (Boron-Titanium), *J. Phase Equilib. Diffus.*, 2006, **27**, p 303
34. A.I. Gusev, Phase Equilibria in the Ternary System Titanium-Boron-Carbon: The Sections TiC<sub>y</sub>-TiB<sub>2</sub> and B<sub>4</sub>C<sub>y</sub>-TiB<sub>2</sub>, *J. Solid State Chem.*, 1997, **133**, p 205-210
35. F. Thévenot, Boron Carbide—A Comprehensive Review, *J. Eur. Ceram. Soc.*, 1990, **6**, p 205-225
36. A. Grytsiv and P. Rogl, Aluminium – Boron – Carbon, *Refractory Metal Systems*, G. Effenberg and S. Ilyenko, Ed., Springer, Berlin, Heidelberg, 2009, p 10-38
37. G. Will, On the Crystal Structure of AlB<sub>10</sub>, *J. Am. Chem. Soc.*, 1963, **85**, p 2335-2336
38. V.I. Matkovich, J. Economy, and R.F. Giese, Presence of Carbon in Aluminum Borides, *J. Am. Chem. Soc.*, 1964, **86**, p 2337-2340
39. V. Raghavan, Al-B-Ti (Aluminum-Boron-Titanium), *J. Phase Equilib. Diffus.*, 2005, **26**, p 173-174
40. J.C. Viala, J. Bouix, G. Gonzalez, and C. Esnouf, Chemical Reactivity of Aluminium with Boron Carbide, *J. Mater. Sci.*, 1997, **32**, p 4559-4573
41. V.T. Witusiewicz, A.A. Bondar, U. Hecht, J. Zollinger, L.V. Artyukh, and T.Y. Velikanova, The Al–B–Nb–Ti System: V. Thermodynamic Description of the Ternary System Al-B-Ti, *J. Alloy. Compd.*, 2009, **474**, p 86-104
42. J. Rodríguez-Carvajal, Recent Advances in Magnetic Structure Determination by Neutron Powder Diffraction, *Phys. B*, 1993, **192**, p 55-69
43. H. Li, S. Li, X. Chen, and Y. Zhou, Spontaneous Pulverisation of Al<sub>4</sub>C<sub>3</sub> Containing MAX Bulk Ceramics at Room Temperature, *Adv. Appl. Ceram.*, 2014, **113**, p 184-188
44. D.C. Halverson, A.J. Pyzik, I.A. Aksay, and W.E. Snowden, Processing of Boron Carbide-Aluminum Composites, *J. Am. Ceram. Soc.*, 1989, **72**, p 775-780
45. Z. Zhang, X.-G. Chen, and A. Charette, Fluidity and Microstructure of an Al-10% B<sub>4</sub>C Composite, *J. Mater. Sci.*, 2009, **44**, p 492-501
46. N. Dhokey, S. Ghule, K. Rane, and R. Ranade, Effect of KBF<sub>4</sub> and K<sub>2</sub>TiF<sub>6</sub> on Precipitation Kinetics of TiB<sub>2</sub> in Aluminium Matrix Composite, *J. Adv. Mater. Lett.*, 2011, **2**, p 210-216
47. S. Zhang, Y. Zhao, G. Chen, X. Cheng, C. She, X. Wang, and D. Wu, Effects of In Situ TiB<sub>2</sub> Particle on Microstructures and Mechanical Properties of AZ91 Alloy, *J. Alloy. Compd.*, 2010, **494**, p 94-97
48. J. Zhang, J. Lee, Y. Cho, S. Kim, and H. Yu, Effect of the Ti/B<sub>4</sub>C Mole Ratio on the Reaction Products and Reaction Mechanism in an Al-Ti-B<sub>4</sub>C Powder Mixture, *Mater. Chem. Phys.*, 2014, **147**, p 925-933